PCCP

PAPER

View Article Online
View Journal | View Issue

Cite this: *Phys. Chem. Chem. Phys.*, 2014, **16**, 25969

Spectroscopic characterization of the interaction of lithium with thin films of the ionic liquid 1-octyl-3-methylimidazolium bis(trifluoromethylsulfonyl)amide†

Mark Olschewski,[a] René Gustus,[a] Marcel Marschewski,[b] Oliver Höfft*[a] and Frank Endres*[a]

Received 14th July 2014,
Accepted 22nd October 2014

DOI: 10.1039/c4cp03091e

www.rsc.org/pccp

In this experimental investigation the interaction of lithium with 1-octyl-3-methylimidazolium bis-(trifluoromethylsulfonyl)amide ([OMIm]Tf_2N) is shown. For this purpose thin films of lithium and [OMIm]Tf_2N were successively vapor deposited on a copper substrate and analyzed by X-ray Photoelectron Spectroscopy (XPS) as well as by Ultraviolet Photoelectron Spectroscopy (UPS). When [OMIm]Tf_2N is evaporated on top of a thin lithium film a chemical shift analysis of XPS spectra shows a variety of reaction products like LiF, Li_2O and Li_xCH_y which reveals the instability of the IL against lithium. Time resolved XPS spectra were discussed to distinguish cation reactions from beam damage effects. In a second step lithium is deposited on a [OMIm]Tf_2N layer. The XPS spectra are in agreement with the results of the previous step, but show some differences concerning the [OMIm] cation. In a third step [OMIm]Tf_2N has been deposited on a passivated lithium layer. XPS results show nearly unaffected $[Tf_2N]^-$ anions and partially decomposed $[OMIm]^+$ cations. Interestingly the cation reactions show similarities when compared to the interaction of [C_4C_1Pyrr]Tf_2N (1-butyl-1-methylpyrrolidinium bis[trifluoromethylsulfonyl]amide) and lithium.

Introduction

Room-temperature ionic liquids (RT-ILs) are of fundamental interest as organic solvents and functionalized materials, as they have a couple of impressive chemical and physical properties.[1–3] Due to their quite low vapor pressure at room temperature, they can be analyzed under vacuum conditions enabling a variety of surface sensitive analysis methods.[4–6] As RT-ILs exhibit good ion conductivities, high temperature stability and a large electrochemical window together with a good solubility for lithium salts, they are of potential interest as electrolyte for non flammable Li based batteries,[7–9] like *e.g.* lithium/air batteries.

Lithium ion batteries are preferentially used for energy storage in cell phones, laptop computers and nowadays in some electrically powered cars. As their energy density is only $\sim$150 W h kg^{-1} and as LiPo batteries are flammable, further development is needed.

Especially fires of lithium ion batteries in e-cars recently attracted the public interest as the commonly used organic solvents for the cells are also volatile and flammable, implying some danger for the driver and rescuers in the case of an accident. Furthermore organic solvents are reactive against metallic lithium, thus lithium anodes, which would enable even higher energy densities,[10,11] are practically excluded with conventional electrolytes.

The variety of possible combinations of anions and cations allows modifying the electrolyte properties precisely. Replacing the organic solvents by ionic liquids has been widely tested and promises to be a good compromise between performance, safety and stability.[12–14]

The interaction of lithium with organic solvents for battery applications like tetrahydrofuran (THF) and propylene carbonate (PC) has been done for instance by Zhuang *et al.*[15] They evaporated thin films of THF and PC in a UHV chamber on a lithium layer and observed a lithium induced decomposition of the organic molecules by using photoelectron spectroscopy (XPS). In the present paper the stability of 1-octyl-3-methylimidazolium bis(trifluoromethylsulfonyl)amide ([OMIm]Tf_2N) against lithium has been investigated by vapor depositing a thin film of the RT-IL on top of a lithium covered copper substrate. The interactions have been analyzed by photoelectron spectroscopy using Al K_α radiation to observe elemental composition as well as chemical state information and He I radiation for valence band spectra of the sample.

[a] *Institute of Electrochemistry, Clausthal University of Technology, Arnold-Sommerfeld-Str 6, D-38678 Clausthal-Zellerfeld, Germany. E-mail: frank.endres@tu-clausthal.de, o.hoefft@pe.tu-clausthal.de*
[b] *Institut für Energieforschung und Physikalische Technologien, Technische Universität Clausthal, Leibnizstrasse 4, D-38678 Clausthal-Zellerfeld, Germany*

† Electronic supplementary information (ESI) available. See DOI: 10.1039/c4cp03091e

In a second step lithium has been deposited on a $[OMIm]Tf_2N$ layer as this might change reaction kinetics or even show differences based on the formation of passivating layers of the reaction products. Beyond that $[OMIm]Tf_2N$ is deposited on a previously oxidized lithium layer in a third step.

As Keppler *et al.* observed degradation of $[EMIm]Tf_2N$ during non monochromatic X-ray irradiation[16] it is important to distinguish beam damage related effects in the interaction of lithium and $[OMIm]Tf_2N$ from those occurring immediately after deposition. Therefore the measurements were evaluated with respect to the irradiation time.

Experimental

The experimental investigations as well as the preparation steps were performed in an UHV chamber with a base pressure of below 5×10^{-10} mbar. A polished copper foil, commonly used as current collector in battery applications,[17] was used as substrate, fixed on a molybdenum sample holder and transferred into the UHV chamber.

For each of the experiments the substrate was cleaned referring to the literature:[18] it was heated by a resistive sample heater (PBN) as part of the Omicron manipulator to 880 K for 10 minutes and etched at this temperature for 10 minutes by argon ions with a kinetic energy of 2 keV using an Omicron ISE 5 ion source. Afterwards, it was heated to 930 K for 15 to 20 minutes, depending on the base pressure in the main chamber. The purity of the copper surface was verified by XPS survey spectra (see ESI†).

The ionic liquid 1-octyl-3-methylimidazolium bis(trifluoromethylsulfonyl)amide ($[OMIm]Tf_2N$) was purchased in the highest available quality (NMR: purity >99%, IC: Halides <100 ppm) from Io-Li-Tec (Germany) and dried under vacuum conditions at 375 K to remove the water content to below 2 ppm.

To produce a thin layer of $[OMIm]Tf_2N$, the RT-IL was evaporated at 415 K for 600 seconds using the TCE-BSC (Kentax GmbH) evaporator resulting in a layer thickness of about 7 nm on top of the substrate, which was validated by XPS intensity loss of the Cu $2p_{3/2}$ peak after deposition. Evaporation of $[OMIm]Tf_2N$ in thin films on Au(111) under UHV conditions has been well investigated.[19,20] The ionic liquid remains intact as thermal decomposition first can be observed in a temperature range above 600 K.[21]

For lithium evaporation a lithium-metal alloy (Alvasources® AS-3-Li-10-C by Alvatec) was heated *via* resistive heating with a current of 8 A resulting in a temperature of about 875 K. At this temperature pure lithium is emitted from the alloy, which is stored in a stainless steel tube. Lithium was vapor deposited for 180 seconds in all experiments described here. The amount of lithium can be estimated by evaporating lithium on the substrate and calculating the thickness by XPS measurements with approx. 0.6 nm. As we expect a difference in the interaction of lithium with the ionic liquid when lithium is previously deposited on the substrate and followed by evaporation of $[OMIm]Tf_2N$ compared to the opposite procedure, this investigation includes three experimental steps:

(1) Depositing $[OMIm]Tf_2N$ on a layer of Li

(2) Depositing Li on a layer of $[OMIm]Tf_2N$

(3) Depositing $[OMIm]Tf_2N$ on a layer of previously oxidized lithium

The steps were characterized by valence band spectroscopy (UPS) using an He I VUV source (Omicron HIS 13) with 21.2 eV photon energy and core level spectroscopy (XPS) using Al K_α radiation with 1486.6 eV photon energy of a non monochromatic X-ray source (Omicron DAR 400).

While the sample is grounded for the XPS measurements, a potential of 5 V was applied for the UPS experiments supporting the emission of low energy electrons. Electrons emitted were detected by a hemispherical analyzer (Omicron EA125) under an angle of 45° to the surface normal.

Since degradation of ionic liquids with imidazolium cations, that are exposed to non-monochromatic X-ray radiation, was observed before,[16] XPS analysis was performed as fast detail scan of the C 1s, N 1s, O 1s, F 1s, S 2p and Li 1s regions with a total exposure time of about 1 h.

As X-ray degradation is a continuous process relative to the exposure time, the beam damage based reaction products can be emphasized by evaluating detail spectra time resolved. For the time resolved XPS plots a 5 data point wide moving average procedure has been applied to time and energy information of fast detail scans.

All spectra were displayed as a function of the binding energy with respect to the Fermi level. The XPS spectra have been charge corrected by fixing the F 1s component of the CF_3 group at 688.5 eV to improve comparability of the results.

For quantitative XPS analysis, a Shirley-background-subtraction was employed.[22] Photoelectron peak areas were calculated by fitting Gauss-type profiles optimized by the Levenberg–Marquard algorithm with the CasaXPS software. Photoelectric cross-sections calculated by Scofield[23] and asymmetry factors calculated by Yeh and Lindau[24] as well as the transmission function of the hemispherical analyzer have been taken into account for stoichiometric calculations. The free mean path of the electrons in organic samples was also involved in the calculations, according to literature.[25]

Results

1. Reference spectrum of $[OMIm]Tf_2N$ on Cu

In Fig. 1–5 detail XPS spectra of the C 1s, N 1s, F 1s and O 1s regions are shown. For a better comparability the intensity of the different experimental parts is scaled equally in each figure. The binding energy (BE) and the relative amount of the fitted component peaks are displayed in Table 1. As the signal/noise ratio of the S 2p peak is rather bad, it has not been taken into account and thus is not displayed here. In the first row (a) of the figures the spectra for $[OMIm]Tf_2N$ as deposited on the copper substrate are shown.

Due to the strong C–F_3 bond the C 1s peak of the anion at 292.8 eV is clearly distinguished from the cation peaks at 286.4 eV and 284.8 eV. While the first cation component at 286.4 eV is associated with carbon atoms in the imidazolium structure in a

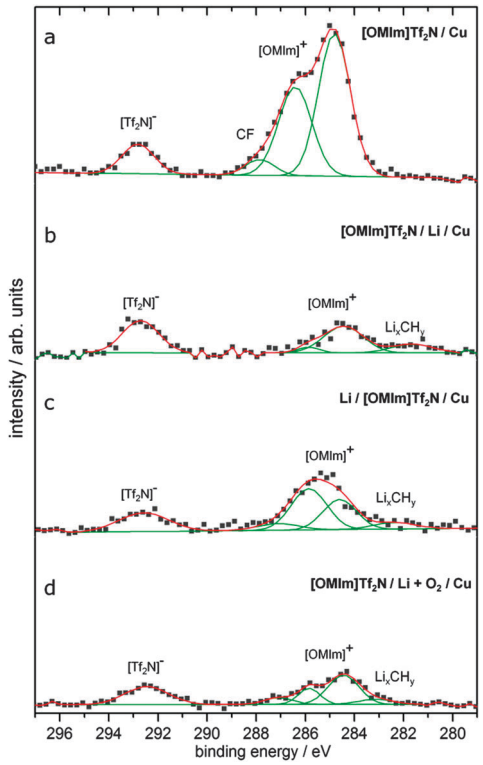

Fig. 1 C 1s XPS spectra for – (a) pure $[OMIm]Tf_2N$ on copper, (b) $[OMIm]Tf_2N$ deposited on a lithium layer, (c) lithium deposited on a $[OMIm]Tf_2N$ layer, (d) $[OMIm]Tf_2N$ deposited on Li_2O.

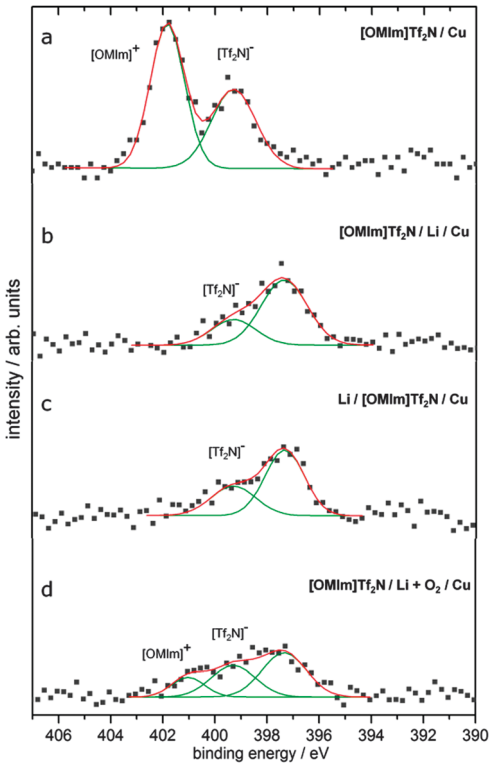

Fig. 2 N 1s XPS spectra for – (a) pure $[OMIm]Tf_2N$ on copper, (b) $[OMIm]Tf_2N$ deposited on a lithium layer, (c) lithium deposited on a $[OMIm]Tf_2N$ layer, (d) $[OMIm]Tf_2N$ deposited on Li_2O.

Table 1 XPS C 1s, N 1s, O 1s and F 1s binding energies and stoichiometry for pure $[OMIm]Tf_2N$ on copper, $[OMIm]Tf_2N$ deposited on a lithium layer, lithium deposited on a $[OMIm]Tf_2N$ layer, $[OMIm]Tf_2N$ deposited on Li_2O

	$[OMIm]Tf_2N$		$[OMIm]Tf_2N$/Li		Li/$[OMIm]Tf_2N$		$[OMIm]Tf_2N$/Li_2O	
Peak	BE [eV]	at%	BE [eV]	at%	BE [eV]	at%	BE [eV]	at%
C 1s			281.7	13	282.4	7	283.1	8
	284.8	51	284.5	39	284.6	25	284.5	37
	286.4	33	285.9	4	285.9	37	285.9	15
	287.9	5			287.1	7	287.1	8
	292.8	11	292.7	43	292.6	24	292.5	32
N 1s			397.4	73	397.3	66	397.4	49
	399.3	41	399.3	27	399.3	34	399.3	35
	401.8	59					401.0	16
O 1s			528.1	16	528.5	28	528.1	25
	530.5	12					530.5	10
			531.2	16	531.2	31	531.2	17
	532.4	88	532.4	68	532.4	41	532.4	48
F 1s			684.8	25	684.9	33	684.8	7
	688.5	100	688.5	75	688.5	67	688.5	93

chemical environment of nitrogen the second component at 284.8 eV is associated with the residual carbon in imidazolium and in the octyl-chain.[26]

The small peak at 287.9 eV can be assigned to C–F[27] which may be associated with radiation induced decomposition of the anion.

The N 1s spectrum in Fig. 2a can as well be divided into two components, as the nitrogen in the cation is more positive compared to the nitrogen in the anion. The first peak at 401.8 eV is related to the $[OMIm]^+$ cation while the second peak at 399.3 eV nitrogen peak is related to $[Tf_2N]^-$.[26]

The spectrum in Fig. 3a shows the O 1s component of the anion peak of $[OMIm]Tf_2N$ at 532.4 eV next to a rather small peak at 530.5 eV. The small peak is a hint for oxidation of the copper substrate either by oxygen impurities during evaporation or by decomposed anions.

In Fig. 4a the XPS spectrum of the F 1s region is displayed. It consists of a single peak at 688.5 eV that can be assigned to carbon in the CF_3 component of the anion.

Due to the high reactivity of copper the interactions of RT-ILs with the copper substrate have to be well considered. Uhl *et al.* recently reported about changes of $[C_4C_1Pyrr]Tf_2N$ (1-butyl-1-methylpyrrolidinium bis[trifluoromethylsulfonyl]amide) vapor deposited in a sub-monolayer film on a Cu(111) surface at room temperature.[28] They observed decomposition of the $[Tf_2N]^-$ anion and found a stable adsorbate phase mainly containing Cu_xS but as well adsorbed CF_3, while the cation remains intact.

Thus the C–F assigned peak in the C 1s spectrum and the small peak in the O 1s spectrum might show radiation based anion decomposition[16] but might as well be based on anion degradation in presence of the copper surface. However, as the present XPS results for $[OMIm]Tf_2N$ on copper are in good agreement with XPS studies in the literature[26,29–31] and as there are no further chemical changes visible, bulk interactions between $[OMIm]Tf_2N$ and copper can be neglected.

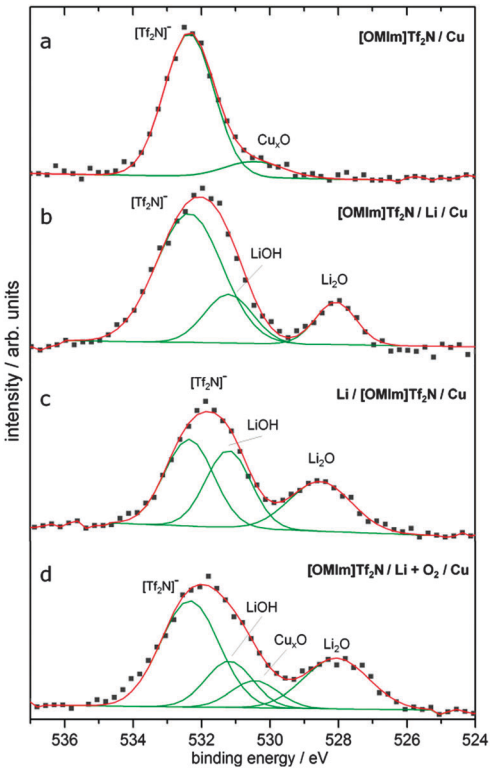

Fig. 3 O 1s XPS spectra for – (a) pure [OMIm]Tf_2N on copper, (b) [OMIm]Tf_2N deposited on a lithium layer, (c) lithium deposited on a [OMIm]Tf_2N layer, (d) [OMIm]Tf_2N deposited on Li_2O.

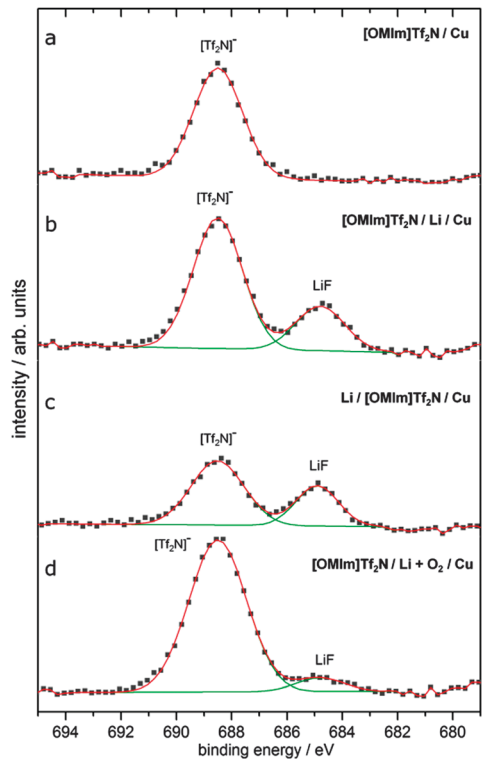

Fig. 4 F 1s XPS spectra for – (a) pure [OMIm]Tf_2N on copper, (b) [OMIm]Tf_2N deposited on a lithium layer, (c) lithium deposited on a [OMIm]Tf_2N layer, (d) [OMIm]Tf_2N deposited on Li_2O.

2. [OMIm]Tf_2N/Li/Cu

When [OMIm]Tf_2N is deposited on a lithium layer major changes can be observed for the cation components in the C 1s (Fig. 1b) and N 1s region (Fig. 2b).

The C 1s peaks of the cation lose about 84% of their peak area and both shift by approx. 0.5 eV to lower binding energies to 285.9 eV and 284.5 eV. In contrast the peak area of the anion peak in the C 1s region at 292.7 eV does not significantly change.

At 281.7 eV a new component shows up in the region where we would expect carbon bound to lithium. The lithium seems to have reacted with the carbon either in the imidazolium ring or in the aliphatic chain to build Li_xCH_y. The peak assignment to Li_xCH_y is in good agreement with the lithium carbon bounds observed for powdered methyllithium and dilithiomethane samples by Meyers *et al.*[32]

In the N 1s region the cation component at 401.8 eV has vanished completely, while the anion component still is located at 399.3 eV. Additionally a new component is detected at 397.4 eV, which is difficult to allocate without doubt as it could either be related to decomposed $[OMIm]^+$ cations or decomposed $[Tf_2N]^-$ anions. However, this peak most likely originates from nitrogen in $[OMIm]^+$ shifted by 4.4 eV to lower binding energies. This means the nitrogen is under these conditions in a completely different chemical environment compared to nitrogen in the imidazolium ring and thus the cation character of $[OMIm]^+$ is lost during the interaction with Li.

The $[Tf_2N]^-$ peak in the O 1s region (Fig. 3b) exhibits a shoulder peak on the low binding energy side at 531.2 eV which is related to reaction products of lithium and [OMIm]Tf_2N. In this region of O 1s we expect Li_2CO_3, but as well LiOH like shown in XPS studies at the electrode surface of non ionic liquid based lithium ion batteries.[33,34]

Additionally a new peak appears at 528.1 eV with a peak area of 16 at% of the total O 1s area, which can be assigned to oxygen in Li_2O.[33–35]

The F 1s spectrum in Fig. 4b also shows a new component at 684.8 eV referring to LiF.[36]

We can conclude that both anion and cation react with the lithium layer. As these reactions might be influenced by beam damage under the incidence of X-ray radiation, we did time dependent measurements. Fig. 5 and 6 display time resolved XPS spectra of the F 1s and C 1s region in a waterfall plot. For reasons of clarity and comparability the first recorded spectrum is fitted and displayed like the spectra in Fig. 1–4, while the other ones are displayed as solid line. For a more detailed view the area of each peak fit is plot in relation to the measurement time in ESI† (Fig. S2).

Fig. 5 clearly shows a continuous decay of the F 1s anion peak at 688.5 eV while the F 1s peak of LiF at 684.8 eV increases. Thus the LiF forms because of beam damage on the anion side. However, as it is already present at the moment where the measurement starts we have to conclude that the initial presence of LiF is due to the reaction of the IL layer with lithium.

The anion peak in the C 1s spectrum (Fig. 6) at 292.7 eV is in good agreement with this. While its peak area continuously decays

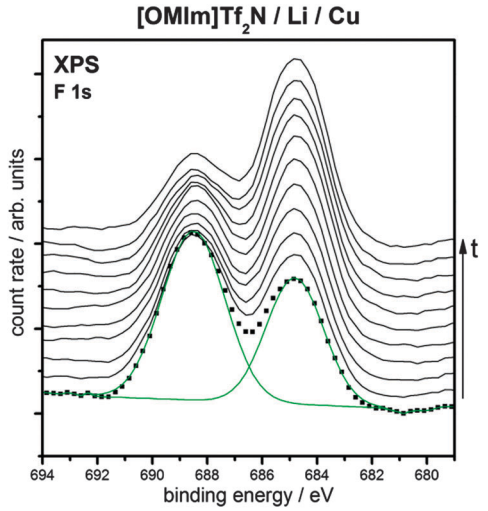

Fig. 5 Waterfall plot of F 1s XPS spectra for [OMIm]Tf_2N deposited on lithium with rising measurement time.

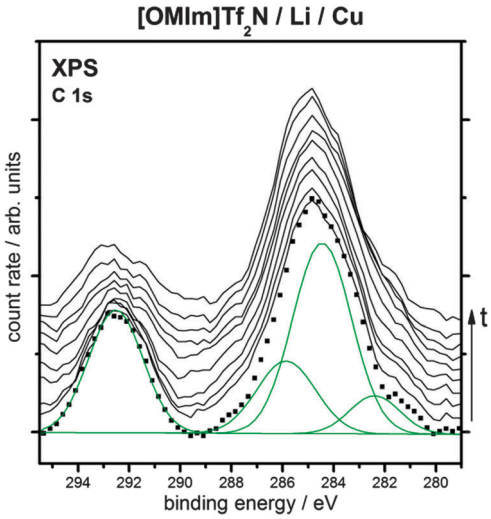

Fig. 6 Waterfall plot of C 1s XPS spectra for [OMIm]Tf_2N deposited on lithium with rising measurement time.

no significant change can be seen for the cation peaks at 285.9 eV and 284.5 eV, as well as for the Li_xCH_y component. Even the N 1s spectrum (see ESI†) does not change with time of measurement. This means the cation reaction must have taken place before the XPS analysis started and the decomposition is not induced by the XPS measurements.

Comparing the C 1s and F 1s spectra in Fig. 5 and 6 with the ones in Fig. 1b and 4b the anion seems to be more strongly reacting with the lithium surface in the waterfall plots (small intensity in the C 1s anion component, great amount of LiF). This most likely is related to the changed order of measurement, may as well be due to partially oxidation of the lithium surface before evaporating [OMIm]Tf_2N.

3. Li/[OMIm]Tf_2N/Cu

When evaporating lithium on a [OMIm]Tf_2N layer the reaction products are quite similar to those observed before. Major differences were observed for the C 1s region in Fig. 1c. The anion peak at 292.6 eV has broadened and is much smaller compared to the peak in step 2 (Fig. 1b). However the relative amount of the anion component in C 1s is still high, compared to the [OMIm]Tf_2N spectrum in the reference (Fig. 1a). The main difference can be detected in the C 1s cation peaks as the component at 285.9 eV, assigned to C–N, raised compared to the result in step 2 (Fig. 1b), thus even exceeds the amount of the C–C component. Maybe this is due to the formation of C–O contributions, which would not be distinguishable from C–N bonds in the shown C 1s XPS spectrum.

The shoulder on the low binding energy side of the C 1s cation peak indicates the existence of Li_xCH_y (ref. 29) and can be fit by a peak at 282.4 eV with an area of 7 at% of the total peak area of the C 1s region.

The N 1s spectrum in Fig. 2c is in good agreement with the results of [OMIm]Tf_2N deposited on a lithium layer shown in step 2 (Fig. 2b). The anion peak can be detected at 399.3 eV, while there is a component at 397.3 eV again, which might be related to reaction products of $[OMIm]^+$ and lithium.

Small changes are observed for the anion peaks of the O 1s and F 1s spectra. The O 1s spectrum in Fig. 3c shows a shoulder peak at 531.2 eV next to the $[Tf_2N]^-$ peak at 532.4 eV, like observed before in step 2. At 528.5 eV a new component has built, which might be Li_2O shifted 0.4 eV to higher binding energies. Compared to [OMIm]Tf_2N evaporated on a lithium layer (step 2) the total intensity of the O 1s anion peak decreased.

A similar trend is observed at the anion peak in the F 1s region in Fig. 4c as its peak area decreased compared to the spectrum in step 2. The area of the LiF component of F 1s at 684.9 eV increased to 33% of the whole F 1s peak area.

4. [OMIm]Tf_2N/Li_2O/Cu

The formation of Li_2O surfaces by an interaction of oxygen with a lithium multilayer has been investigated by Shek *et al.*[37] Referring to their work a lithium layer was oxidized by exposure of approx. 10 L O_2. The formation of a Li_2O surface has been verified by UPS spectra and XPS analysis of the O 1s peak. Next to the Li_2O peak the O 1s spectrum after O_2 exposure exhibits a smaller peak, which may be associated with partial oxidation of the copper surface. Thus the lithium layer might either not be completely closed or there is oxygen diffusion through the lithium layer.

As for the results shown above in step 2 and step 3 (Fig. 1b and c), the C 1s component of the anion in Fig. 1d is intense compared to the cation peaks. However, the $[OMIm]^+$ peak with its components at 284.5 eV and 285.9 eV is shaped like the reference peak in step 1 (Fig. 1a). Additionally there is a small component at 283.1 eV BE which is correlated to Li_xCH_y,[32] like already observed for the previous experiments. The small shoulder peak in the C 1s spectrum at 287.1 eV on the high binding energy side of the cation peak could be explained by C–F fragments of decomposed anion.

In Fig. 2d the N 1s spectrum of [OMIm]Tf_2N evaporated on an oxidized lithium layer is shown. There are three peaks visible in the N 1s region. The peaks at 397.4 eV and 399.3 eV are in

good agreement with the components shown in step 2 and step 3 (Fig. 2b and c). Compared to them the peak area and thus the amount of nitrogen of the new component at 397.4 eV is decreased.

Additionally there is another component at 401.0 eV which most probably is related to nitrogen in $[OMIm]^+$. The shift of the N 1s peak by 0.8 eV to lower binding energies, compared to the $[OMIm]^+$ component in the reference, can be explained by a slightly modified chemical environment and is in good agreement with XPS spectra of neutral imidazolium compared to cationic ones[38] and spectra of RT-ILs with imidazolium cations in general.[26,29]

When $[OMIm]Tf_2N$ is deposited on top of the Li_2O layer the O 1s spectrum (Fig. 3d) shows 4 different peaks. On the one hand the peaks of Li_2O at 528.1 eV and Cu_xO at 530.5 eV, which already have been measured before evaporating $[OMIm]Tf_2N$, on the other hand the O 1s peak of $[Tf_2N]^-$ at 532.4 eV and the shoulder peak at 531.2 eV, which both can be fit analog to steps 2 and 3 (see Fig. 3b and c). Remarkably the shoulder peak has 17% of the whole O 1s peak area, thus Li_2O might be reduced in the reaction with $[OMIm]Tf_2N$.

In contrast the F 1s spectrum in Fig. 4d is clearly dominated by the fluorine in the CF_3 component of the anion. The LiF component at 684.8 eV is quite small with a peak area of 7% of the sum of both F 1s component areas.

Li 1s. For each of the experiments Li 1s can be detected in the region between 54 eV and 58 eV. The resulting Li 1s spectra after reaction of lithium and $[OMIm]Tf_2N$ are shown in Fig. 7. Due to the very low photoionization cross section of the Li 1s state, long integration times have to be chosen to observe this peak in more detail. As this would enhance the decomposition of the ionic liquid and possibly lead to side reactions, a bad signal/noise ratio has to be taken into account here.

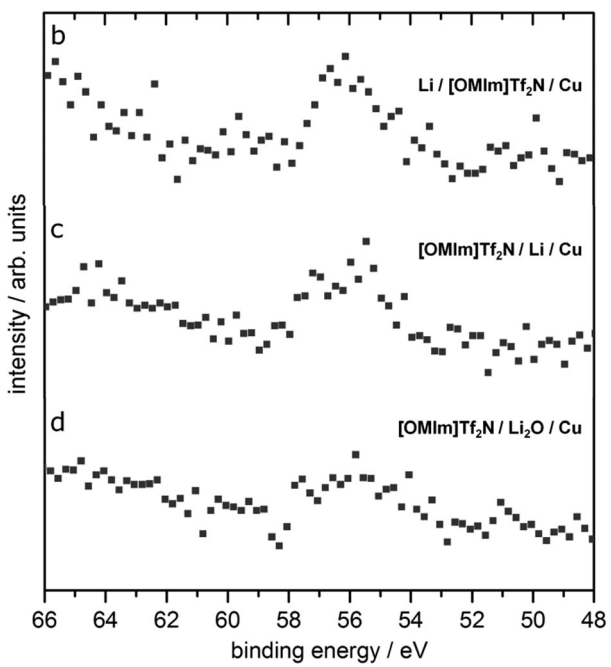

Fig. 7 Li 1s XPS spectra for – (b) $[OMIm]Tf_2N$ deposited on a lithium layer, (c) lithium deposited on a $[OMIm]Tf_2N$ layer, (d) $[OMIm]Tf_2N$ deposited on Li_2O.

UPS results. In addition to the XPS results UPS spectra were recorded (see ESI†) for $[OMIm]Tf_2N$ deposited on Li and on Li_2O immediately after sample preparation. With increasing time after deposition the two main peaks of the RT-IL[30,39] decrease continuously, which could be caused by desorption of the ionic liquid or by rearrangement of the components and has not been observed before.[20] Further experiments are needed to interpret these UPS results in detail. In the case of $[OMIm]Tf_2N$ evaporated on top of the lithium layer contributions of LiF and Li_2O appear next to the main peaks of the RT-IL, which is in good agreement with the XPS results. When evaporated on top of the oxidized lithium layer no additional features can be observed next to a small Li_2O peak and the main peaks of $[OMIm]Tf_2N$.

Discussion

The experiments exhibit an instability of $[OMIm]Tf_2N$ against lithium. As shown in the time-resolved XPS spectra in Fig. 5 and 6 some of the species observed formed during the measurement, *i.e.* caused by the incidence of X-rays.

A fragmentation of the $[Tf_2N]^-$ anion by electrons was shown in literature before.[40,41] Whishart *et al.* observed the degradation pathways of different ILs by electron paramagnetic resonance spectroscopy and predicted a charge transfer process of the much more stable cation radicals to the anion.[40] Keppler *et al.* have shown similar anion fragmentation and desorption occurring on slow time-scales when exposed to X-ray radiation, which most probably is the reason for the formation of LiF and Li_2O during the measurements in the presence of lithium.[16]

However, as the time-resolved XPS spectra in Fig. 5 exhibit a certain amount of LiF even in the first spectrum, the reactions of $[Tf_2N]$ and lithium initially started before XPS analysis. This is in good agreement with the few observations on lithium ion batteries using ionic liquids with $[Tf_2N]^-$ anion as electrolyte.[42,43]

$[C_4C_1Pyrr]Tf_2N$

The decomposition of the cation in the presence of lithium is subject to a different process, as the cation peaks of the N 1s and C 1s regions do not change during XPS analysis. To investigate the role of the imidazolium cation in the reaction, experiments with ionic liquids with alternative cations have to be performed and compared to these results.

As a first insight Fig. 8 and 9 show the C 1s and N 1s spectra of $[C_4C_1Pyrr]Tf_2N$ (1-butyl-1-methylpyrrolidinium bis[trifluoromethylsulfonyl]amide) deposited on copper and on lithium/copper, similar to the experiments above. The XPS spectra of ionic liquids with pyrrolidinium ions have been well described by Men *et al.*[44] As those spectra are in good agreement with the present results interactions of $[C_4C_1Pyrr]Tf_2N$ with copper, recently observed for sub-monolayers,[28] might have a minor effect on thicker RT-IL films.

Due to the different chemical environment of carbon bound to nitrogen the carbon in the cation C 1s spectrum in Fig. 8 can

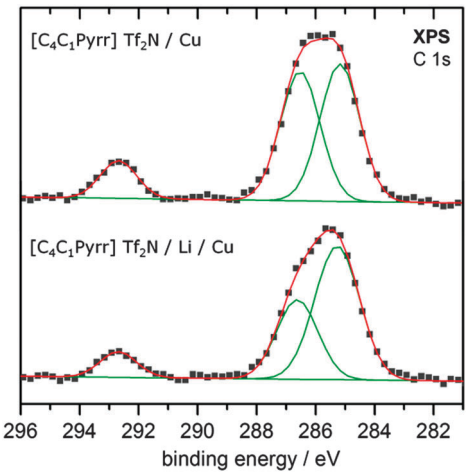

Fig. 8 C 1s XPS spectra for $[C_4C_1Pyrr]Tf_2N$ deposited on copper (top) and on a lithium layer (bottom).

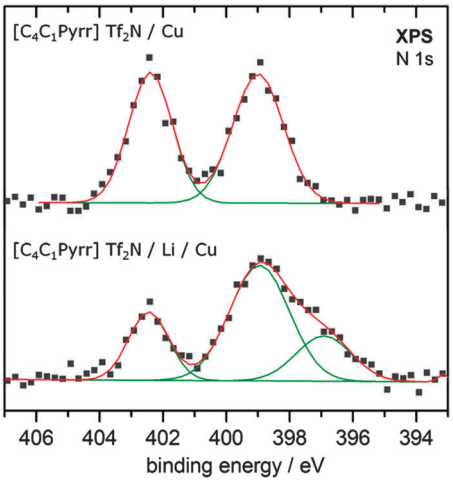

Fig. 9 N1s XPS spectra for $[C_4C_1Pyrr]Tf_2N$ deposited on copper (top) and on a lithium layer (bottom).

be divided in C–C and C–N components, too. If $[C_4C_1Pyrr]Tf_2N$ is evaporated on lithium, the intensity of the second peak (here at 286.5 eV) associated with carbon in a nitrogen electronic environment decreases, while the peak area of the other components remains nearly constant. The peak area of the N 1s cation peak (at 402.4 eV) in Fig. 9 decreases when the RT-IL is evaporated on lithium, in good agreement to the C 1s spectra. Additionally a new component has formed at 396.9 eV analog to the results observed for N 1s in $[OMIm]Tf_2N$ (see Fig. 2).

Howlett *et al.* analysed the solid electrolyte interface of a cycled lithium/copper electrode using $[C_4C_1Pyrr]Tf_2N$ as electrolyte.[42] They observed the presence of reduction products of $[Tf_2N]^-$ on the electrode interface, in good agreement with the anion reaction products shown before. Although a certain influence of the cation was noted, the role of $[C_4C_1Pyrr]^+$ in the reaction remains ambiguous. Interestingly also a new component in the N 1s XPS spectrum was found on the low binding energy side after interaction with lithium, which is supposed to be nitride and part of the native film of the *ex situ* prepared sample.

In our case no nitrogen contamination was observed during sample preparation (see survey spectra in ESI†). On the contrary Fig. 9 shows the formation of a new nitrogen species concomitant with partially decomposition of $[C_4C_1Pyrr]^+$. This most likely is based on a breakup of the pyrrolidinium structure changing the local chemical environment of nitrogen to a chain-like LiC_xH_yN structure.

Nguyen *et al.* investigated the SEI during lithiation of a silicon–copper electrode covered with $[C_3C_1Pyrr]Tf_2N$ using FTIR spectroscopy and XPS.[45] They observed degradation of anion and cation depending on the applied voltage and cleavage of C–F bonds in the $[Tf_2N]^-$ anion responsible for LiF formation. In the N 1s region of the XPS results a new peak is detected with a similar binding energy shift, which is supposed to be related with further degradation products of the anion after cleavage of the C–F bond.

On the contrary Weingarth *et al.* performed an *in situ* electrochemical XPS study for $[EMIm]BF_4$ on platinum and observed the formation of a new peak at this position in the N 1s region, which is a clear evidence for an imidazolium cation decomposed and fragments adsorbed on the electrode surface.[46]

As N 1s spectra of $[C_4C_1Pyrr]Tf_2N$ and $[OMIm]Tf_2N$, each in interaction with lithium, show similarities concerning the cation region (compare with Fig. 2b–d), breakup of the imidazolium structure most probably is the reason for the changes of the cation peaks in steps 2–4, too. But as both decomposed Tf_2N anions[45] and decomposed imidazolium cations[46] result in an N 1s component around 397.4 eV this cannot be proven here.

Nevertheless, quite similar results with XPS have been obtained for tetrahydrofuran and propylene carbonate by Zhuang. *et al.*[15] Both organic molecules react with the lithium layer and were decomposed. The authors claim the decomposition is based on ring-opening, too. In addition they found desorption of fragments of the decomposed molecules into the vacuum at elevated temperatures.

Furthermore Zhao *et al.* observed changes in the XPS cation peaks of $[EMIm]Tf_2N$, which is used as electrolyte for lithium secondary batteries, after cycling. Those changes as well were reported to involve breakup of the imidazolium ring and are quite similar to the present results.[47]

For a slight impression of the mechanisms behind Valencia *et al.* performed *ab initio* calculations of $[EMIm]BF_4$ adsorbed on crystalline lithium surfaces.[48] They observed a great attraction of lithium to the $[BF_4]^-$ anion together with the partial reduction of $[EMIm]^+$.

But as Li_xCH_y components and most probably C–O compounds can be observed in the results here, the decomposition of $[OMIm]^+$ cation might be more complex and proceeding in several steps. Especially the differences in the cation components of the C 1s spectra (Fig. 1) of $[OMIm]Tf_2N$ deposited on lithium and lithium deposited on a $[OMIm]Tf_2N$ layer are unclear at this state. As the intensity and peak area ratio of the N 1s peaks (Fig. 2) of both experiments are in good agreement, carbon species of decomposed $[OMIm]^+$ most likely were involved in the reaction with lithium. This furthermore would

explain the shoulder peak in the O 1s spectrum, which could not be explained by anion decomposition. However the peaks would not be distinguishable from the peaks of $[OMIm]Tf_2N$ in the C 1s and O 1s spectra, thus further experiments are needed.

The results of the UPS spectra indicate a loss of $[OMIm]Tf_2N$ or its components in the interaction with lithium or Li_2O (see ESI†). This is emphasized by loss of intensity in the XPS peaks, mainly in C 1s cation peaks, and supports the conclusion most of the cations or more likely parts of decomposed cations were desorbed in presence of lithium on the copper surface.

As loss of fragments from X-ray induced degraded imidazolium cations using mass spectroscopy has been observed before[16] thermal desorption spectroscopy (TDS) measurements of ionic liquids on a lithium surface could help out identifying desorbed species and thus might explain the decomposition of $[OMIm]^+$ in presence of lithium in more detail.

Passivation of the lithium surface slows down or even prevents the interaction of $[OMIm]Tf_2N$ and lithium. This is obvious comparing the peak area of the LiF species in the F 1s spectra (Fig. 4b–d). The highest amount of LiF with 33% can be found for lithium deposited on top of $[OMIm]Tf_2N$. The amount of LiF when $[OMIm]Tf_2N$ is deposited on a previously oxidized lithium layer is only 7% of the total F 1s peak area. In this case even the cation does not decompose completely. When lithium is evaporated first followed by evaporation of $[OMIm]Tf_2N$ there might be a passivation of the lithium surface by the reaction products leading to a lower amount of LiF and Li_2O.

Conclusion

In the current paper the reaction of the ionic liquid $[OMIm]Tf_2N$ with Li and Li_2O has been investigated. Both the cation and the anion react with lithium, giving a series of decomposition products like Li_xCH_y, Li_2O and LiF. Time resolved XPS measurements show that species like LiF and Li_2O continuously form during the measurement. However, as these species were already present at the moment where the XPS measurement has started it is excluded that they solely form during the measurement, thus they must initially be the result of a chemical reaction of $[OMIm]^+$ with lithium. Interestingly, the cation C 1s and N 1s spectra show similarities when compared to the first results obtained for the interaction of $[C_4C_1Pyrr]Tf_2N$ with lithium.

The results give a first insight into the reaction products that have to be expected when $[OMIm]Tf_2N$ and other ionic liquids with an imidazolium cation shall be used either as electrolyte or additive in lithium ion batteries. In our next steps we will thus investigate how liquids with pyrrolidinium cations interact with lithium or sodium in more detail.

Acknowledgements

This work was supported within the post graduate programme ''Graduiertenkolleg Energiespeicher und Elektromobilität Niedersachsen'' (GEENI) by the Federal Ministry of Science and Culture in Lower Saxony.

References

1 K. Binnemans, *Chem. Rev.*, 2005, **105**, 4148–4204.
2 F. Endres and S. Zein El Abedin, *Phys. Chem. Chem. Phys.*, 2006, **8**, 2101.
3 C. Pinilla, M. G. Del Pópolo, R. M. Lynden-Bell and J. Kohanoff, *J. Phys. Chem. B*, 2005, **109**, 17922–17927.
4 K. Kanai, T. Nishi, T. Iwahashi, Y. Ouchi, K. Seki, Y. Harada and S. Shin, *J. Electron. Spectrosc. Relat. Phenom.*, 2009, **174**, 110–115.
5 V. Lockett, R. Sedev, C. Bassell and J. Ralston, *Phys. Chem. Chem. Phys.*, 2008, **10**, 1330.
6 D. Yoshimura, T. Yokoyama, T. Nishi, H. Ishii, R. Ozawa, H. Hamaguchi and K. Seki, *J. Electron. Spectrosc. Relat. Phenom.*, 2005, **144–147**, 319–322.
7 D. Ensling, M. Stjerndahl, A. Nytén, T. Gustafsson and J. O. Thomas, *J. Mater. Chem.*, 2008, **19**, 82.
8 H. Sakaebe and H. Matsumoto, *Electrochem. Commun.*, 2003, **5**, 594–598.
9 M. Ishikawa, T. Sugimoto, M. Kikuta, E. Ishiko and M. Kono, *J. Power Sources*, 2006, **162**, 658–662.
10 H. Sakaebe, H. Matsumoto and K. Tatsumi, *J. Power Sources*, 2005, **146**, 693–697.
11 H. Matsumoto, H. Sakaebe, K. Tatsumi, M. Kikuta, E. Ishiko and M. Kono, *J. Power Sources*, 2006, **160**, 1308–1313.
12 F. F. Bazito, Y. Kawano and R. M. Torresi, *Electrochim. Acta*, 2007, **52**, 6427–6437.
13 M. Armand, F. Endres, D. R. MacFarlane, H. Ohno and B. Scrosati, *Nat. Mater.*, 2009, **8**, 621–629.
14 A. Lewandowski and A. Świderska-Mocek, *J. Power Sources*, 2009, **194**, 601–609.
15 G. Zhuang, K. Wang and P. N. Ross, *Surf. Sci.*, 1997, **387**, 199–212.
16 A. Keppler, M. Himmerlich, T. Ikari, M. Marschewski, E. Pachomow, O. Höfft, W. Maus-Friedrichs, F. Endres and S. Krischok, *Phys. Chem. Chem. Phys.*, 2010, **13**, 1174.
17 J. Shu, M. Shui, F. Huang, D. Xu, Y. Ren, L. Hou, J. Cui and J. Xu, *Electrochim. Acta*, 2011, **56**, 3006–3014.
18 M. Bowker and R. J. Madix, *Surf. Sci.*, 1981, **102**, 542–565.
19 T. Cremer, M. Stark, A. Deyko, H.-P. Steinrück and F. Maier, *Langmuir*, 2011, **27**, 3662–3671.
20 S. Krischok, A. Ulbrich, T. Ikari, V. Kempter, M. Marschewski and O. Höfft, *Nucl. Instrum. Methods Phys. Res., Sect. B*, 2014, DOI: 10.1016/j.nimb.2014.07.036.
21 S. Zhang, N. Sun, X. He, X. Lu and X. Zhang, *J. Phys. Chem. Ref. Data*, 2006, **35**, 1475.
22 D. Shirley, *Phys. Rev. B: Solid State*, 1972, **5**, 4709–4714.
23 J. H. Scofield, *J. Electron. Spectrosc. Relat. Phenom.*, 1976, **8**, 129–137.
24 J. J. Yeh and I. Lindau, *At. Data Nucl. Data Tables*, 1985, **32**, 1–155.
25 R. F. Roberts, D. L. Allara, C. A. Pryde, D. N. E. Buchanan and N. D. Hobbins, *Surf. Interface Anal.*, 1980, **2**, 5–10.
26 K. R. J. Lovelock, I. J. Villar-Garcia, F. Maier, H.-P. Steinrück and P. Licence, *Chem. Rev.*, 2010, **110**, 5158–5190.

27 C. Cardinaud, *J. Electrochem. Soc.*, 1988, **135**, 1472.
28 B. Uhl, F. Buchner, S. Gabler, M. Bozorgchenani and R. Jürgen Behm, *Chem. Commun.*, 2014, **50**, 8601–8604.
29 H.-P. Steinrück, *Phys. Chem. Chem. Phys.*, 2012, **14**, 5010.
30 T. Ikari, A. Keppler, M. Reinmöller, W. J. D. Beenken, S. Krischok, M. Marschewski, W. Maus-Friedrichs, O. Höfft and F. Endres, *e-J. Surf. Sci. Nanotechnol.*, 2010, **8**, 241–245.
31 M. Reinmöller, A. Ulbrich, T. Ikari, J. Preiß, O. Höfft, F. Endres, S. Krischok and W. J. D. Beenken, *Phys. Chem. Chem. Phys.*, 2011, **13**, 19526.
32 G. F. Meyers, M. B. Hall, J. W. Chinn and R. J. Lagow, *J. Am. Chem. Soc.*, 1985, **107**, 1413–1414.
33 Q.-H. Wu, A. Thißen and W. Jaegermann, *Surf. Sci.*, 2005, **578**, 203–212.
34 C. K. Chan, R. Ruffo, S. S. Hong and Y. Cui, *J. Power Sources*, 2009, **189**, 1132–1140.
35 R. Younesi, S. Urbonaite, K. Edström and M. Hahlin, *J. Phys. Chem. C*, 2012, **116**, 20673–20680.
36 S. Kowalczyk, F. McFeely, L. Ley, R. Pollak and D. Shirley, *Phys. Rev. B: Solid State*, 1974, **9**, 3573–3581.
37 M. L. Shek, J. Hrbek, T. K. Sham and G.-Q. Xu, *Surf. Sci.*, 1990, **234**, 324–334.
38 D. Nolting, N. Ottosson, M. Faubel, I. V. Hertel and B. Winter, *J. Am. Chem. Soc.*, 2008, **130**, 8150–8151.
39 O. Höfft, S. Bahr, M. Himmerlich, S. Krischok, J. A. Schaefer and V. Kempter, *Langmuir*, 2006, **22**, 7120–7123.
40 J. F. Wishart, I. A. Shkrob and S. D. Chemerisov, *J. Phys. Chem. B*, 2007, **111**, 11786–11793.
41 G. Chatel, R. Pflieger, E. Naffrechoux, S. I. Nikitenko, J. Suptil, C. Goux-Henry, N. Kardos, B. Andrioletti and M. Draye, *ACS Sustainable Chem. Eng.*, 2013, **1**, 137–143.
42 P. C. Howlett, N. Brack, A. F. Hollenkamp, M. Forsyth and D. R. MacFarlane, *J. Electrochem. Soc.*, 2006, 595–606.
43 C. C. Nguyen and S.-W. Song, *Electrochem. Commun.*, 2010, **12**, 1593–1595.
44 S. Men, B. B. Hurisso, K. R. J. Lovelock and P. Licence, *Phys. Chem. Chem. Phys.*, 2012, **14**, 5229.
45 C. C. Nguyen, S.-W. Woo and S.-W. Song, *J. Phys. Chem. C*, 2012, **116**, 14764–14771.
46 D. Weingarth, A. Foelske-Schmitz, A. Wokaun and R. Kötz, *Electrochem. Commun.*, 2011, **13**, 619–622.
47 L. Zhao, J.-i. Yamaki and M. Egashira, *J. Power Sources*, 2007, **174**, 352–358.
48 H. Valencia, M. Kohyama, S. Tanaka and H. Matsumoto, *Phys. Rev. B: Condens. Matter Mater. Phys.*, 2008, **78**, 205402.